INTERNATIONAL JOURNAL FOR NUMERICAL METHODS IN FLUIDS, VOL. 13, 775–796 (1991)

A PRACTICAL IMPLEMENTATION OF TURBULENCE MODELS FOR THE COMPUTATION OF THREE-DIMENSIONAL SEPARATED FLOWS

YVES P. MARX

Institut de Machines Hydrauliques et de Mécanique des Fluides, Ecole Polytechnique Fédérale de Lausanne, CH-1015 Lausanne, Switzerland

SUMMARY

An upwind MUSCL-type implicit scheme for the three-dimensional Navier–Stokes equations is presented and details on the implementation for three-dimensional flows of a 'diagonal' upwind implicit operator are developed. Turbulence models for separated flows are also described with an emphasis on the numerical specificities of the Johnson–King non-equilibrium model. Good predictions of separated two- and three-dimensional flows are demonstrated.

KEY WORDS Compressible viscous flows Implicit methods Upwind scheme Turbulence modelling

1. INTRODUCTION

During the late 1970s to the mid 1980s, numerical methods for solving the Euler and Navier–Stokes equations have been extensively developed: acceleration techniques were improved by the introduction of implicit[1] or multigrid[2] schemes; shock waves were also better captured with either an *ad hoc* added artificial dissipation[3] or with new high-order upwind schemes.[4,5] Many computations performed in the late 1980s showed clearly that these techniques are reasonably efficient to solve the two-dimensional Navier–Stokes equations. These techniques are currently being extended to compute realistic flows on complex three-dimensional geometries. The codes developed can also serve to test the predictability of turbulent models on three-dimensional configurations. In the present work, one such test is described. Emphasis is given to practical details, such as the three-dimensional extension of an implicit 'diagonal' upwind method, and on the implementation of a non-equilibrium turbulence model. These details, which are usually overlooked, proved in practice to be important since they are often the limit between failure and success. The outline of the work is the following. After a short description of the equations to be solved (Section 2), the numerical procedure is detailed: the spatial discretization in Section 3, the time integration and acceleration technique in Section 4 and the boundary conditions in Section 5. The turbulence models used are then described (Section 6) and their numerical behaviour is discussed (Section 7). Finally, in Section 8 results are presented, demonstrating that the main features of three-dimensional separated flows can be predicted.

2. GOVERNING EQUATIONS

The basic equations used to describe the physical model are the integral form of the Reynolds equations. Since the dominant viscous effects for high-Reynolds-number flows arise from the

0271–2091/91/160775–22$11.00

Received June 1990
Revised December 1990

diffusion normal to the body surfaces, the thin layer approximation is employed. The turbulent transport of momentum and energy due to the fluctuations of velocity and pressure is modelled using the eddy viscosity concept, making the form of the Reynolds equations identical to the form of the Navier–Stokes equations. The equations to be solved are then

$$\frac{\partial}{\partial t}\iiint_{\mathscr{V}} U\,dv+\iint_{\partial\mathscr{V}} \mathbf{F}\vec{n}\,ds=\iint_{\partial\mathscr{V}} \mathbf{F}_V\vec{n}\,ds, \tag{1}$$

where

$$U=(\rho, \rho u, \rho v, \rho w, e)^{\mathrm{T}}$$

is the vector of the conserved variables. The quantity $\mathscr{V}$ denotes an arbitrary control volume, while $\partial\mathscr{V}$ and n correspond respectively to the boundary surface and the outer normal of this volume.

In a Cartesian frame $(\vec{i}, \vec{j}, \vec{k})$ the tensor $\mathbf{F}$ of the convection terms is

$$\mathbf{F}=\begin{bmatrix} \rho u & \rho v & \rho w \\ \rho u^2+P & \rho uv & \rho uw \\ \rho uv & \rho v^2+P & \rho vw \\ \rho uw & \rho vw & \rho w^2+P \\ u(e+P) & v(e+P) & w(e+P) \end{bmatrix}, \tag{2}$$

and the tensor $\mathbf{F}_V$ of the diffusion terms in the thin layer approximation in the direction $\vec{\eta}$ is

$$\mathbf{F}_V=\begin{bmatrix} 0 & 0 & 0 \\ \sigma_{xx} & \sigma_{xy} & \sigma_{xz} \\ \sigma_{xy} & \sigma_{yy} & \sigma_{yz} \\ \sigma_{xz} & \sigma_{yz} & \sigma_{zz} \\ u\sigma_{xx}+v\sigma_{xy}+w\sigma_{xz}-q_x & u\sigma_{xy}+v\sigma_{yy}+w\sigma_{yz}-q_y & u\sigma_{xz}+v\sigma_{yz}+w\sigma_{zz}-q_z \end{bmatrix}. \tag{3}$$

with

$$\sigma_{xx}=\lambda\left(\eta_x\frac{\partial u}{\partial\eta}+\eta_y\frac{\partial v}{\partial\eta}+\eta_z\frac{\partial w}{\partial\eta}\right)+\mu\left(2\eta_x\frac{\partial u}{\partial\eta}\right),$$

$$\sigma_{yy}=\lambda\left(\eta_x\frac{\partial u}{\partial\eta}+\eta_y\frac{\partial v}{\partial\eta}+\eta_z\frac{\partial w}{\partial\eta}\right)+\mu\left(2\eta_y\frac{\partial v}{\partial\eta}\right),$$

$$\sigma_{zz}=\lambda\left(\eta_x\frac{\partial u}{\partial\eta}+\eta_y\frac{\partial v}{\partial\eta}+\eta_z\frac{\partial w}{\partial\eta}\right)+\mu\left(2\eta_z\frac{\partial w}{\partial\eta}\right),$$

$$\sigma_{xy}=\mu\left(\eta_y\frac{\partial u}{\partial\eta}+\eta_x\frac{\partial v}{\partial\eta}\right),\qquad \sigma_{xz}=\mu\left(\eta_z\frac{\partial u}{\partial\eta}+\eta_x\frac{\partial w}{\partial\eta}\right),\qquad \sigma_{yz}=\mu\left(\eta_z\frac{\partial v}{\partial\eta}+\eta_y\frac{\partial w}{\partial\eta}\right),$$

$$q_x=-\frac{\gamma\mu}{Pr}\eta_x\frac{\partial e_i}{\partial\eta},\qquad q_y=-\frac{\gamma\mu}{Pr}\eta_y\frac{\partial e_i}{\partial\eta},\qquad q_z=-\frac{\gamma\mu}{Pr}\eta_z\frac{\partial e_i}{\partial\eta},$$

where e_i represents the internal energy. The bulk viscosity λ is evaluated using the Stokes hypothesis

$$3\lambda+2\mu=0,$$

and the molecular viscosity is determined from the Sutherland law

$$\mu=\mu_\infty\left(\frac{T}{T_\infty}\right)^{3/2}\frac{T_\infty+110{\cdot}4}{T+110{\cdot}4}. \tag{4}$$

As a result of the eddy viscosity assumption, equations (1) with expression (3) for the tensor $\mathbf{F}_V$ correspond also to the Reynolds equations for turbulent flows if the molecular viscosity is replace by an 'effective' viscosity $\mu+\mu_t$ and the quantity μ/Pr by $\mu/Pr+\mu_t/Pr_t$. The symbols μ_t and Pr_t used in the previous expressions denote respectively the eddy viscosity and the turbulent Prandtl number.

3. NUMERICAL METHOD

Equations (1) are solved with an implicit upwind method of the form

$$(I+\Delta t\,\mathrm{L})\delta U=-\Delta t\,\mathrm{R}^n, \qquad U^{n+1}=U^n+\delta U, \tag{5}$$

where I is the identity matrix, L is a spatial operator and R is the residual of the steady equations. Since in this work we are interested only in the steady solution of (1), no accuracy restriction is imposed on the implicit operator L.

3.1. Computation of the residual

The computation of the residual is performed following the idea introduced by Godunov[6] and generalized by Van Leer.[7] The procedure comprises three stages. The first stage consists of the *reconstruction* of the flow field from its cell-averaged values by piecewise polynomial approximations. In the second stage, the time *evolution* of the reconstructed flow field is computed by solving at each cell face a Riemann problem. The procedure is therefore 'upwind' since the wave propagation is taken into account when the Riemann problem is solved. In the final stage the solution obtained by the resolution of the Riemann problems is *projected* on the cells and new average values are computed. This step makes the overall procedure conservative. In the numerical procedure used, the computation of the residual corresponds also to the explicit step as opposed to the implicit step which corresponds to the inversion of the operator $I+\Delta t\,\mathrm{L}$.

3.2. Reconstruction scheme

The reconstruction of the flow field at each cell face is performed using the κ-scheme, wherein the left (L) and right (R) values at the $i+\frac{1}{2}$ cell faces are computed with an upwind-biased interpolation:

$$q_{\mathrm{L}i+1/2}=\bar{q}_i+\frac{h_i}{2}[(1+\kappa)\delta\bar{q}_{i+1/2}+(1-\kappa)\delta\bar{q}_{i-1/2}],$$

$$q_{\mathrm{R}i+1/2}=\bar{q}_{i+1}-\frac{h_{i+1}}{2}[(1+\kappa)\delta\bar{q}_{i+1/2}+(1-\kappa)\delta\bar{q}_{i+3/2}], \tag{6}$$

with

$$\delta\bar{q}_{i+1/2}=\frac{\bar{q}_{i+1}-\bar{q}_i}{h_{i+1}+h_i}.$$

In the above equation, h_i represents the distance between the $i+\frac{1}{2}$ and $i-\frac{1}{2}$ face centres, q is any conservative variable and an overbar indicates a cell-averaged quantity. For $\kappa \in [-1, 1]$ the κ-scheme is second-order-accurate and stable. The particular value $\kappa=\frac{1}{3}$ leads even to a third-order-accurate scheme (on a uniform one-dimensional mesh).

In order to ensure an interpolation that does not increase the total variation of the initial distribution, the gradients $\delta\bar{q}$ have to be limited. Following Reference 8, the gradients were limited by replacing $\delta\bar{q}$ by $\tilde{\delta}$, with

$$\tilde{\delta}_i^+ = \text{minmod}\left[\frac{\bar{q}_{i+1}-\bar{q}_i}{h_{i+1}+h_i}, b\frac{\bar{q}_i-\bar{q}_{i-1}}{h_i+h_{i-1}}\right], \qquad \tilde{\delta}_i^- = \text{minmod}\left[\frac{\bar{q}_i-\bar{q}_{i-1}}{h_i+h_{i-1}}, b\frac{\bar{q}_{i+1}-\bar{q}_i}{h_{i+1}+h_i}\right],$$

where the 'minmod' operator is defined by

$$\text{minmod}(x, y)=\begin{cases}\text{sign}(x)\min(|x|, |y|) & \text{if } \text{sign}(x)=\text{sign}(y),\\ 0 & \text{otherwise.}\end{cases}$$

The value of b corresponds to the largest value for which the interpolated $q_{i+1/2}$ lies between $\bar{q}_i$ and $\bar{q}_{i+1}$:

$$b=\frac{3-\kappa}{1-\kappa}.$$

The cell face values are thus computed with

$$q_{\text{L}i+1/2}=\bar{q}_i+\frac{h_i}{2}[(1+\kappa)\tilde{\delta}_i^+ +(1-\kappa)\tilde{\delta}_i^-],$$

$$q_{\text{R}i+1/2}=\bar{q}_{i+1}-\frac{h_{i+1}}{2}[(1+\kappa)\tilde{\delta}_{i+1}^- +(1-\kappa)\tilde{\delta}_{i+1}^+]. \tag{7}$$

3.3. Resolution of the Riemann problem

In the original work of Godunov the Riemann problems were solved exactly, but it has been proven that the same flow fields could be obtained at a lower cost if the Riemann problems were solved only approximately. Two such approximate Riemann solvers are those proposed by Roe[5] and Osher.[4] They both rely on wave decomposition. In this work the Roe Riemann solver is employed because it requires less computing time and leads essentially to the same solution as the Osher Riemann solver.[9] If the left and right states at a cell face are U_{L} and U_{R}, the wave decomposition used in the Roe scheme is made by assuming a locally constant state $\tilde{U}$ for which

$$U_{\text{R}}-U_{\text{L}}=\sum_k \tilde{r}_k\tilde{\alpha}_k, \qquad F(U_{\text{R}})-F(U_{\text{L}})=\sum_k \tilde{\lambda}_k\tilde{r}_k\tilde{\alpha}_k, \tag{8}$$

where $\tilde{\lambda}_k$ is an eigenvalue of the Jacobian matrix $\partial F(\tilde{U})/\partial U$, $\tilde{r}_k$ is a right eigenvector of $\partial F(\tilde{U})/\partial U$ and $\tilde{\alpha}_k=\tilde{l}_k(U_{\text{R}}-U_{\text{L}})$, with $\tilde{l}_k$ a left eigenvector of $\partial F(\tilde{U})/\partial U$.

In Reference 10 it is shown that the state $\tilde{U}$ for which equations (8) are satisfied exists and is unique. It can be computed using the special averaging introduced by Roe.[5]

The flux at the cell face is then computed using

$$F_{i+1/2}=F(U_{\text{L}})+\sum_k \Delta F_k^-, \tag{9}$$

where ΔF^- is defined as

$$\Delta F_k^- = \tilde{\lambda}_k^- \tilde{r}_k\tilde{\alpha}_k, \tag{10}$$

and with

$$\lambda^- = \frac{\lambda - |\lambda|}{2}.$$

The above expressions are useful for computations in a Cartesian mesh. For general meshes the wave decomposition is made in the direction normal to the cell face. Such a choice is computationally convenient but is also quite arbitrary because the decomposition depends on the mesh rather than on the flow properties. In practice, however, the procedure appears to perform well and most of the codes based on upwind discretization use this decomposition. With the 'grid-splitting' procedure the extension to generalized co-ordinates of the approximate Riemann solvers is simple: the Cartesian velocities u, v and w have just to be replaced by the contravariant velocities $\check{u}$, $\check{v}$ and $\check{w}$,

$$\check{u} = n_x u + n_y v + n_z w, \qquad \check{v} = l_x u + l_y v + l_z w, \qquad \check{w} = m_x u + m_y v + m_z w, \tag{11}$$

where $\vec{n}$ is the vector normal to the cell face and $\vec{l}$ and $\vec{m}$ are the tangential vectors. In the two-dimensional case the tangential vector is uniquely defined by the knowledge of the normal vector; in the three-dimensional case the normal vector defines only a *family* of tangential vectors $\vec{l}$ and $\vec{m}$. A precise definition of these tangential vectors can, however, be avoided by noticing that only the linear combinations of the tangential velocities,

$$\Omega_x = l_x \check{v} + m_x \check{w}, \qquad \Omega_y = l_y \check{v} + m_y \check{w}, \qquad \Omega_z = l_z \check{v} + m_z \check{w},$$

are needed and that these linear combinations can also be written as

$$\Omega_x = u - n_x \check{u}, \qquad \Omega_y = v - n_y \check{u}, \qquad \Omega_z = w - n_z \check{u}. \tag{12}$$

Thus, in order to avoid a precise definition of the tangential vectors, the tangential velocities $\check{v}$ and $\check{w}$ are replaced in the computations by the velocities Ω_x, Ω_y and Ω_z.

3.4. Computation of the viscous terms

In a finite volume approach the computation of the viscous terms requires the evaluation of first-order derivatives at the cell faces. The computation of such gradients may be obtained using the Gauss theorem, but in this work a simpler procedure is employed. The gradients are computed with

$$\frac{\partial q_{i+1/2}}{\partial \xi} = 2 \frac{(q_{i+1} - q_i)\mathscr{S}_{i+1/2}}{\mathscr{V}_{i+1} + \mathscr{V}_i}, \tag{13}$$

where $\mathscr{S}_{i+1/2}$ is the surface of the interface and $\mathscr{V}_i$ and $\mathscr{V}_{i+1}$ are the volumes of the cells on the two sides of the interface.

4. IMPLICIT OPERATOR

The implicit operator used to accelerate convergence to steady state is an extension of the operator presented by Coakley.[11] It is derived from a backward Euler implicit integration of equation (1). Instead of solving this operator by relaxation techniques as done in two dimensions[12-14] and, partially, in three dimensions,[15] the three-dimensional implicit operator is

dimensionally split,[1] leading to the resolution of three one-dimensional operators of the form

$$\left(I+\Delta t\frac{\partial \check{A}}{\partial \xi}-\Delta t\frac{\partial M}{\partial \xi}\frac{\partial}{\partial \xi}\right)\delta U=\text{RHS}, \tag{14}$$

where $\check{A}$, the Jacobian matrix of the Euler flux in the curvilinear co-ordinate ξ (having the vector normal to the cell face $\vec{n}=n_x\vec{i}+n_y\vec{j}+n_z\vec{k}$ as the directional vector), is given by

$$\check{A}=\frac{\partial F}{\partial U}n_x+\frac{\partial G}{\partial U}n_y+\frac{\partial H}{\partial U}n_z,$$

with

$$F=\mathbf{F}\vec{i}, \qquad G=\mathbf{F}\vec{j}, \qquad H=\mathbf{F}\vec{k}.$$

In (14) M is the matrix of the viscous terms.

If the spatial derivatives of (14) are discretized with a three-point stencil, the resolution of system (14) necessitates the inversion of 5×5 block tridiagonal matrix. Following Chaussee and Pulliam,[16] the system can be 'diagonalized', leading to the inversion of scalar tridiagonal systems. This is accomplished by first replacing the matrix M by its spectral radius σI. The Jacobian matrix $\check{A}$ is then decomposed as $\check{A}=T^{-1}\check{\Lambda}T$ (where T is the matrix of the left eigenvectors of $\check{A}$ and $\check{\Lambda}$ is the diagonal matrix of the eigenvalues) and the product $T^{-1}\check{\Lambda}$ is taken out of the spatial derivative $\partial/\partial\xi$. Introducing the characteristic variables $\delta\check{U}=T\delta U$ and multiplying equation (14) by the matrix T, the system to be solved becomes

$$\left(I+\Delta t\check{\Lambda}\frac{\partial}{\partial \xi}-\Delta t\sigma I\frac{\partial^2}{\partial \xi^2}\right)\delta\check{U}=\text{RHS}. \tag{15}$$

The Coakley scheme is finally obtained if a first-order upwind approximation is used for the spatial derivatives of the convective terms and a centred approximation for the diffusion terms. It should be noted that whereas the matrix $\check{A}$ involves only the components of the normal vector $\vec{n}$, the matrices T^{-1}, T and thereafter $\delta\check{U}$ involve also the tangential vectors $\vec{l}$ and $\vec{m}$. As a consequence, while the original system requires only the knowledge of the normal vector $\vec{n}$, the 'diagonalized' system necessitates also the definition of the tangential vectors $\vec{l}$ and $\vec{m}$. Since the normal vector $\vec{n}$ is calculated by taking the cross product $\vec{t}_1\times\vec{t}_2$ (Figure 1), it seems natural to

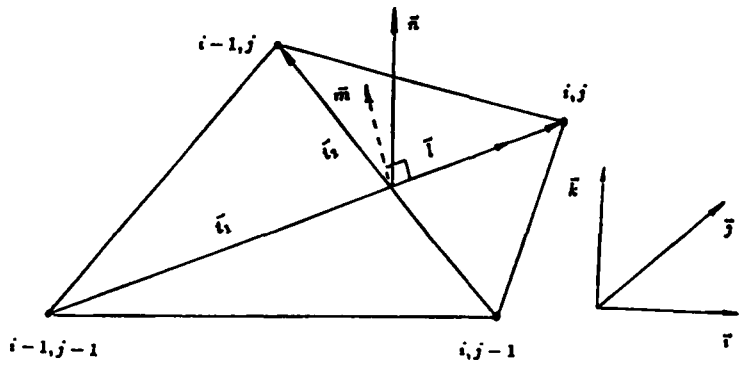

Figure 1. Definition of the cell face reference frame

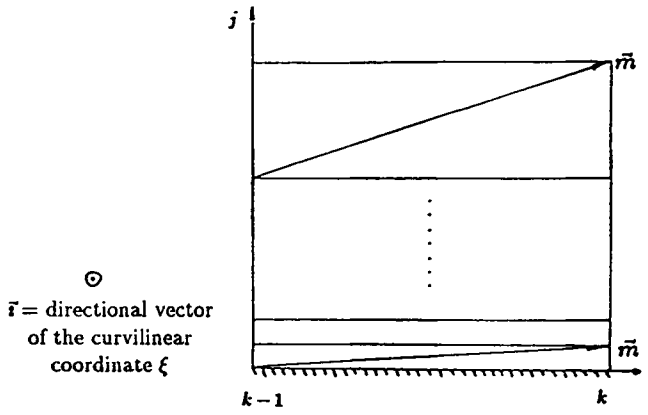

Figure 2. Evolution of the tangential vector $\vec{m}$ in the boundary layer

choose

$$\vec{l}=\frac{\vec{t}_1}{\|\vec{t}_1\|}, \tag{16}$$

$$\vec{m}=\vec{n}\times\vec{l}. \tag{17}$$

Such a procedure, however, produces spurious crossflows for purely two-dimensional flows. In the simple case of a two-dimensional turbulent flow on a flate plate, the vectors $\vec{j}$ and $\vec{k}$ can be chosen as the tangential vectors if the mesh is Cartesian (Figure 2). The contravariant velocities are then identical to the Cartesian velocities.

$$\Delta\check{u}=\Delta u, \qquad \Delta\check{v}=\Delta v, \qquad \Delta\check{w}=\Delta w\ (=0),$$

and the implicit system for the tangential velocities can be written as

$$\mathscr{L}[\delta v]_i=[\Delta v]_i, \qquad \mathscr{L}[\delta w]_i=[\Delta w]_i, \tag{18}$$

where Δq and δq denotes an increment computed after the explicit step and after the implicit step respectively and $[q]_i$ is the vector of the variables q_j defined in the plane $i=$constant:

$$[\delta q]_i=[\delta q_{i,1},\ldots,\delta q_{i,j-1},\delta q_{i,j},\delta q_{i,j+1}\ldots,\delta q_{i,J}]^{\mathrm{T}}.$$

If the matrix $\mathscr{L}$ is not singular, spurious crossflow cannot be introduced by the implicit operator.

When equations (16) and (17) are used to compute the tangential vectors $\vec{l}$ and $\vec{m}$, the tangential vectors will differ from $\vec{j}$ and $\vec{k}$. In any plane $i=$constant their form will be

$$\vec{l}_j=\alpha_j\vec{j}+\beta_j\vec{k}, \qquad \vec{m}_j=\gamma_j\vec{j}+\delta_j\vec{k}.$$

Using these vectors for the definition of the contravariant velocities, the 'diagonal' implicit system can be written

$$\mathscr{L}[\delta\check{v}]_i=[\alpha][\Delta v]_i+[\beta][\Delta w]_i, \qquad \mathscr{L}[\delta\check{w}]_i=[\gamma][\Delta v]_i+[\delta][\Delta w]_i;$$

thus

$$[\delta\check{v}]_i=\mathscr{L}^{-1}[\alpha][\Delta v]_i+\mathscr{L}^{-1}[\beta][\Delta w]_i, \qquad [\delta\check{w}]_i=\mathscr{L}^{-1}[\gamma][\Delta v]_i+\mathscr{L}^{-1}[\delta][\Delta w]_i. \tag{19}$$

The solution of the implicit operator will be independent of the choice of the tangential vectors if the tangential velocities also satisfy

$$[\delta\check{v}]_i=[\alpha][\delta v]_i+[\beta][\delta w]_i, \qquad [\delta\check{w}]_i=[\gamma][\delta v]_i+[\delta][\delta w]_i. \tag{20}$$

Unfortunately, relations (20) are not always fulfilled, as can be seen by replacing, in (19), $\mathscr{L}[\delta v]_i$ for $[\Delta v]_i$ and $\mathscr{L}[\delta w]_i$ for $[\Delta w]_i$:

$$\begin{aligned}[\delta\check{v}]_i&=\mathscr{L}^{-1}[\alpha]\mathscr{L}[\delta v]_i+\mathscr{L}^{-1}[\beta]\mathscr{L}[\delta w]_i,\\ [\delta\check{w}]_i&=\mathscr{L}^{-1}[\gamma]\mathscr{L}[\delta v]_i+\mathscr{L}^{-1}[\delta]\mathscr{L}[\delta w]_i.\end{aligned} \tag{21}$$

Expressions (21) are identical to (20) if and only if the matrix $\mathscr{L}$ commutes with the diagonal matrices $[\alpha]$, $[\beta]$, $[\gamma]$ and $[\delta]$. For general matrices $\mathscr{L}$ it is then required that

$$[\alpha]=\alpha I, \qquad [\beta]=\beta I, \qquad [\gamma]=\gamma I, \qquad [\delta]=\delta I. \tag{22}$$

In the case of the two-dimensional turbulent flow on the flate plate, because of the stretching of the mesh in the boundary layer, relations (22) are far from being satisfied and, as a consequence, a strong crossflow is generated ($\delta w\neq 0$). What appears to be the 'natural' procedure should therefore be rejected.

The method proposed to compute the tangential velocities—which avoids a precise definition of the tangential vectors $\vec{l}$ and $\vec{m}$—follows the procedure used in the explicit step: the computation of the increments of the tangential velocity vectors $\delta\check{v}$ and $\delta\check{w}$ is replaced by

$$\begin{aligned}\delta\Omega_x&=(l_x\delta\check{v}+m_x\delta\check{w})=\delta u-n_x\delta\check{u},\\ \delta\Omega_y&=(l_y\delta\check{v}+m_y\delta\check{w})=\delta v-n_y\delta\check{u},\\ \delta\Omega_z&=(l_z\delta\check{v}+m_z\delta\check{w})=\delta w-n_z\delta\check{u}.\end{aligned} \tag{23}$$

Performing linear combinations on the equations for $\delta\check{v}$ and $\delta\check{w}$, the following equations are obtained:

$$\delta\Omega_\theta+\check{u}\Delta t\left(l_\theta\frac{\partial\delta\check{v}}{\partial\xi}+m_\theta\frac{\partial\delta\check{w}}{\partial\xi}\right)=\Delta\Omega_\theta, \quad \theta=x, y, z. \tag{24}$$

Finally, neglecting locally the spatial variation of the co-ordinate components l_θ and m_θ, the equations for $\delta\Omega_\theta$ can be formed:

$$\left(I+\check{u}\Delta t\frac{\partial}{\partial\xi}\right)\delta\Omega_\theta=\Delta\Omega_\theta, \quad \theta=x, y, z. \tag{25}$$

Thus, instead of solving the two equations for $\delta\check{v}$ and $\delta\check{w}$, the three equations for $\delta\Omega_x$, $\delta\Omega_y$ and $\delta\Omega_z$ will be solved. The three velocity components $\delta\Omega_\theta$ are not independent; they should satisfy

$$n_x\delta\Omega_x+n_y\delta\Omega_y+n_z\delta\Omega_z=0. \tag{26}$$

Because of the simplification made for the transformation of (24), equation (26) is generally not verified; the tangential vector $\delta\vec{\Omega}$ does not lie in the tangential plane. Therefore it is replaced by its projection on the tangential plane,

$$\delta\Omega'_\theta=\delta\Omega_\theta-n_\theta\delta, \tag{27}$$

with

$$\delta=n_x\delta\Omega_x+n_y\delta\Omega_y+n_z\delta\Omega_z.$$

By construction, no spurious crossflow can be generated with this procedure. Numerical experiments were performed; they confirm that for purely two-dimensional flows the three-dimensional operator leads effectively to the same convergence rate as the corresponding two-dimensional operator.

5. BOUNDARY CONDITIONS

The use of upwind schemes simplifies significantly the computation at the boundaries since only 'physical' boundary conditions are needed. For instance, if only simple waves are assumed at the boundaries, the Osher P-variant scheme can be used at the boundaries by replacing the information contained in the waves outside the computational domain by the natural physical boundary conditions: static pressure at an outflow boundary; rest temperature, rest pressure and flow angle at an inflow; no slip velocity, zero normal pressure gradient and adiabaticity at a solid wall; etc. For lifting aerofoils, the freestream conditions are modified by taking into account the circulation around the aerofoil as discussed in Reference 17. The undisturbed flow conditions are used for flows around finite wings since the disturbances created by the wing decay more rapidly in the three-dimensional case than in the two-dimensional one.

In the implicit step all the boundary conditions are treated implicitly. For the characteristic variables $\delta\Omega_x$, $\delta\Omega_y$, $\delta\Omega_z$ and $a^2\delta\rho-\delta P$, if the index of the boundary is denoted by $N+1$, the equations at all boundaries can be cast into the form

$$\delta U_{N+1}=d_1\delta U_N+d_2\delta U_{N-1}, \tag{28}$$

with

$d_1=d_2=0$	for a solid wall, a far-field boundary,
$d_1=\frac{3}{2}$ and $d_2=-\frac{1}{2}$	for an extrapolated boundary condition,
$d_1=1$ or 0 and $d_2=0$	for a symmetry condition,
⋮	

If treated implicitly, the symmetry and wall boundary conditions introduce some coupling between the variables $\delta R^+=\delta P+\rho a\delta\breve{u}$ and $\delta R^-=\delta P-\rho a\delta\breve{u}$. Therefore the implicit equations cannot be completely decoupled and a 2×2 block tridiagonal system has to be solved for these characteristic variables. The boundary conditions associated with this 2×2 system are the equivalent of (28),

$$\begin{bmatrix}\delta R^+\\ \delta R^-\end{bmatrix}_{N+1}=\begin{bmatrix}d_1^+ & d_2^+\\ d_1^- & d_2^-\end{bmatrix}\begin{bmatrix}\delta R^+\\ \delta R^-\end{bmatrix}_N+\begin{bmatrix}d_3^+ & 0\\ 0 & d_3^-\end{bmatrix}\begin{bmatrix}\delta R^+\\ \delta R^-\end{bmatrix}_{N-1}, \tag{29}$$

with

$d_{1,2,3}^{\pm}=0$	for a far-field boundary,
$d_1^{\pm}=d_2^{\pm}=\frac{1}{2}$ and $d_3^{\pm}=0$	at a wall and a symmetry plane,
$d_1^+=d_2^-=\frac{3}{2}$, $d_2^+=d_1^-=0$ and $d_3^{\pm}=-\frac{1}{2}$	for an extrapolated boundary conditions,
⋮	

Since the same functional form (28) or (29) is used at all types of boundaries, the computation of implicit boundary conditions does not impair the capability for vectorization of the implicit step.

6. TURBULENCE MODELLING

Two simple mixing length turbulence models were examined in this work. The first model considered is the conventional Baldwin–Lomax model[18]

$$\nu_{ti}=\rho K^2\eta^2 D^2|\omega|, \qquad K=0{\cdot}4, \qquad \nu_{to}=1{\cdot}6F_W\,\mathrm{Fkleb}(\eta), \qquad \nu_t=\min(\nu_{ti},\nu_{to}), \tag{30}$$

where

$$D=1-\exp\left(-\frac{\eta^+}{26}\right), \qquad \eta^+=\frac{u_\tau\eta}{\nu}, \qquad u_\tau=\max\sqrt{(\nu\omega)},$$

$$F_W=\min\left[\eta_{max}F_{max},\frac{\eta_{max}(|\check{u}|_{max}-|\check{u}|_{min})^2}{F_{max}}\right],$$

$$F_{max}=\max_j(F(\eta))_{i,j,k}, \qquad F(\eta_{max})=F_{max}, \qquad F(\eta)=\eta|\omega|D,$$

$$\mathrm{Fkleb}(\eta)=0{\cdot}0168\left[1+5{\cdot}5\left(\frac{0{\cdot}3\eta}{\eta_{max}}\right)^6\right]^{-1}.$$

The definition of u_τ has been chosen slightly different from the wall shear stress used in the original Baldwin–Lomax turbulence model. This modification is necessary to enforce $u_\tau>0$. Using the original Baldwin–Lomax formulation, it is possible to find at a separation point that $u_\tau=0$, which then leads to laminar flow, $\nu_t=0$! This can happen when the foot of a mesh line coincides with the location of a saddle separation point, where the vorticity at the wall is zero.

It is well known that equilibrium models such as the Baldwin–Lomax model are not suited for separated flows for which the diffusion and the convection of turbulence are not negligible, since they introduce an imbalance between production and dissipation rates of turbulence. While retaining the eddy viscosity assumption, these non-equilibrium effects can be taken into account by two-equation models, K–ε and K–ω. However, it appears that despite their 'universality', the two-equation models do not improve significantly the agreement between the computed results and the experimental data for separated flows.[19] A less ambitious approach is to modify two-layer mixing length models in order to extend their applicability to separated flows. Such an approach has been taken by Johnson and King, [20] and the model they derived appears to be adequate for the computation of separated flows on aerofoils and wings.[21,19]

The idea behind the Johnson–King model is: (i) to scale the turbulent velocity to the square root of the maximum Reynolds shear stress rather than to the product of the wall vorticity by a length scale; (ii) to compute the maximum Reynolds shear stress by solving a differential equation in which non-equilibrium effects are taken into account. Since the level of the turbulent shear stress is then determined by the differential equation, the Johnson–King model, in contrast to more conventional mixing length models, neither depends only on local mean flow gradients nor assumes a turbulence in equilibrium. The eddy viscosity distribution in the inner layer is

$$\nu_{ti}=K\eta D^2 u_M, \tag{31}$$

where

$$u_M=\left(\frac{\tau_M}{\rho}\right)^{1/2}, \qquad D=1-\exp\left(\frac{-\eta^+}{17}\right), \qquad \eta^+=\frac{\eta\max(u_M,u_\tau)}{\nu}.$$

Here and below the index M indicates the location where the Reynolds shear stress is maximum.

As stated, the turbulent shear stress τ_M is obtained through the resolution of a differential equation; see Reference 20 for its derivation. In the three-dimensional case this equation is

$$\breve{u}_M \frac{\partial}{\partial \xi}\left(\frac{\tau_M}{\rho}\right)^{-1/2} \breve{w}_M \frac{\partial}{\partial \zeta}\left(\frac{\tau_M}{\rho}\right)^{-1/2} = \frac{0{\cdot}125}{L_M}\left[1-\left(\frac{\tau_M}{\tau_{eq}}\right)^{-1/2}+\frac{2L_M}{\delta(0{\cdot}7-\eta/\delta)}|1-\sqrt{\sigma}|\right], \quad (32)$$

with

$$L_M = \min(K\eta_M,\ 0{\cdot}225K\delta).$$

The left-hand side of (32) represents the convection of the turbulent shear stress. The diffusion of the turbulent shear stress is modelled by the last term of the right-hand side, while the remaining term corresponds to the imbalance between the production and dissipation of turbulence. This term is consequently approximated by the difference between the actual shear stress and the shear stress that would have been obtained if turbulence had been in equilibrium. This shear stress τ_{eq} is computed at $\eta = \eta_M$ using

$$\tau_{eq} = \mu_{teq}|\omega|, \qquad \nu_{teq} = \nu_{toeq}\left[1-\exp\left(\frac{\nu_{tieq}}{\nu_{toeq}}\right)\right], \qquad \nu_{tieq} = K\eta D^2 u_{eq}, \qquad \nu_{toeq} = 1{\cdot}6F_W Fk, \quad (33)$$

with

$$D = 1-\exp\left(-\frac{\eta u_{eq}}{17\nu}\right), \quad u_{eq}^2 = \max(\nu_{teq}|\omega|), \quad Fk = 0{\cdot}0168\left[1+5{\cdot}5\left(\frac{\eta}{\delta}\right)^6\right]^{-1}, \quad \delta = 1{\cdot}9\eta_{max}.$$

The convection terms of (32) are approximated by first-order upwind differences. The equation is then solved with a point-alternate symmetric Gauss–Seidel relaxation with one relaxation performed in each direction.

In the original formulation of Johnson and King the outer eddy viscosity layer was based on the Cebeci–Smith distribution. This formulation was well suited in the boundary layer context used by Johnson and King for the derivation of their model. However, for Navier–Stokes codes the Baldwin–Lomax formulation is more convenient since it eliminates the need for finding the edge of the boundary layer, which usually is a source of numerical errors. The outer eddy viscosity layer is therefore calculated using

$$\nu_{to} = \sigma 1{\cdot}6F_W Fk = \sigma \nu_{toeq}. \quad (34)$$

The coefficient σ is introduced to force the value of the maximum shear stress $\tilde{\tau}_M = \max(\mu_t|\omega|)$ to match the value τ_M obtained from the solution of the differential equation (32).

The final value of the eddy viscosity ν_t is then computed from a blending of ν_{ti} and ν_{to}:

$$\nu_t = \nu_{to}\left[1-\exp\left(-\frac{\nu_{ti}}{\nu_{to}}\right)\right]. \quad (35)$$

7. NUMERICAL BEHAVIOUR OF THE JOHNSON–KING MODEL

In this section the behaviour of the Johnson–King model is examined in more detail from a numerical point of view—discussion of the predictions of the model and comparison with experimental data are left to the Results section. Despite its simplicity, the Johnson–King model is highly sensitive to its actual implementation, which usually is not described in detail. The crucial points are (i) the computation of u_{eq}, (ii) the location where to turn on the Johnson–King model and (iii) the computation of σ.

7.1. Computation of u_{eq}

In the following the method for computing u_{eq} is explained such that

$$u_{eq}^2 = \max(\nu_{teq}|\omega(u_{eq})|) \tag{36}$$

is automatically enforced. An explicit expression can be given if ν_{teq} is computed using $\nu_{teq} = \min(\nu_{tieq}, \nu_{toeq})$ instead of $\nu_{teq} = \nu_{toeq}[1 - \exp(-\nu_{tieq}/\nu_{toeq})]$. The latter relation was introduced by Johnson and King for reasons that will be discussed in Section 7.3.

When the maximum of $\nu_{teq}|\omega|$ is located in the inner layer, the value of the eddy viscosity is

$$\nu_{teq} = \nu_{tieq} = KyD^2 u_{eq}.$$

The definition of u_{eq} then leads to

$$u_{eq}^2 = \nu_{tieq}|\omega| = KyD^2 u_{eq}|\omega|,$$

which implies

$$u_{eq} = KyD^2|\omega|. \tag{37}$$

The function $f_i = (KyD^2|\omega|)^2$ is thus the locus of the possible values of u_{eq}^2 when the maximum of $\nu_{teq}|\omega|$ is located in the inner layer. Let us now introduce the points y_{eq2}, y_i and y_o defined by:

(a) y_{eq2} is the point where $f_i(y_{eq2}) = f_o(y_{eq2})$ with $f_o(y) = \nu_{toeq}|\omega(y)|$ (the functions f_i and f_o have always at least one intersection; in cases of multiple intersections, y_{eq2} is the position of the first one)

(b) y_o is the point where $f_o(y)$ is maximum for $y \geqslant y_{eq2}$

(c) y_i is the point where $f_i(y)$ is maximum for $y \leqslant y_{eq2}$.

The value of u_{eq} satisfying (37) is then

$$u_{eq}^2 = \max(f_o(y_o), f_i(y_i)). \tag{38}$$

A graphical representation of the three possible cases is given in Figure 3.

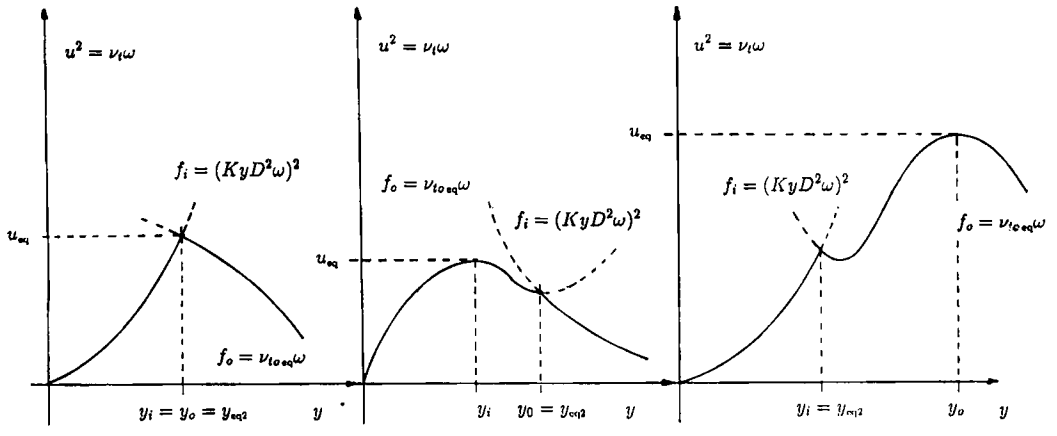

Figure 3. Possible locations for u_{eq}

7.2. Initial conditions for the Johnson–King model

For two-dimensional problems the computation of the maximum shear stress τ_M requires only the solution of one ODE. The solution of the equation can easily be obtained using a marching procedure. However, as with any marching procedure, some initial condition must be supplied. The obvious choice is to compute the turbulent quantities on the first sections after the transition from laminar to turbulent flow with the equilibrium model. The transition from the equilibrium model, equation (33), to the non-equilibrium model, equations (31) and (34), is then located in a region where

$$\frac{\mathrm{d}}{\mathrm{d}\xi}\left(\frac{\tau_{eq}}{\rho}\right)^{-1/2} \simeq 0.$$

This condition appears naturally when replacing, in (32) τ_M by τ_{eq} and σ by one, and is *imperative* in order to have a smooth distribution of the eddy viscosities in the flow field.

7.3. Computation of σ

As explained in the description of the model, the coefficient σ is introduced in order to force the value $\tilde{u}_M^2 = \max(\nu_t|\omega|)$ to be identical to the value $u_M^2 = \tau_M/\rho$ obtained by solving equation (32). If the maximum of $\nu_t|\omega|$ is located in the outer layer and if ν_t is calculated by $\nu_t = \min(\nu_{ti}, \nu_{to})$, than σ is simply

$$\sigma = \frac{u_M^2}{\nu_{to\,eq}|\omega|_M}.$$

The procedure proposed in Reference 21,

$$\sigma^{k+1} = \sigma^k \frac{u_M^2}{\tilde{u}_M^2(\sigma^k)}, \tag{39}$$

gives also in this case the correct solution. This procedure, however, fails when the maximum is located in the inner layer, because it is possible that $\tilde{u}(\sigma^{k+1}) = \tilde{u}(\sigma_k)$ (Figure 4). In the following it is explained how to calculate—in one iteration—the value of σ which enforces $\tilde{u}_M = u_M$. The procedure explaining how to calculate σ will also shed some light on the appearance of situations for which $\sigma \gg 1$ and $\sigma \ll 1$.

The value σ for which $u_M = \tilde{u}_M$ is

$$\sigma = \frac{u_M^2}{\nu_{to\,eq}|\omega|_{y=y_o}}, \tag{40}$$

with y_o defined as the location where $f_o(y)$ is maximum for $y \geqslant y_2$. The function $f_o(y)$ is

$$f_o(y) = \nu_{to\,eq}|\omega|,$$

and the point y_2 is the first point for which $f_i(y) = KyD^2|\omega|^2$ is equal to u_M^2 (the extreme situation where $f_i(y)$ does not intersect u_M^2 will be discussed later). A graphical representation of the correction process (40) is displayed in Figure 5 for usual situations. For these usual situations, σ exists and is unique.

Let us now examine unconventional situations. The first unconventional situation is when $f_i(y)$ and u_M^2 do not intersect. Two cases must be distinguished. The first case is when $y_i < y_o$, where y_i and y_o are the locations for which $f_i(y)$ and $f_o(y)$ respectively are maximum. In this case equation

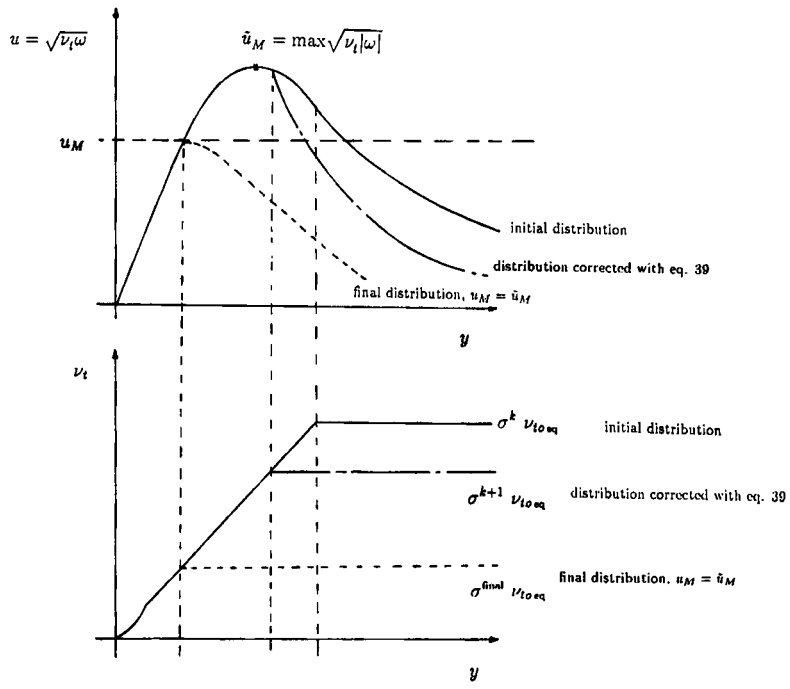

Figure 4. Effect of σ on the velocity scale $\tilde{u}_M$

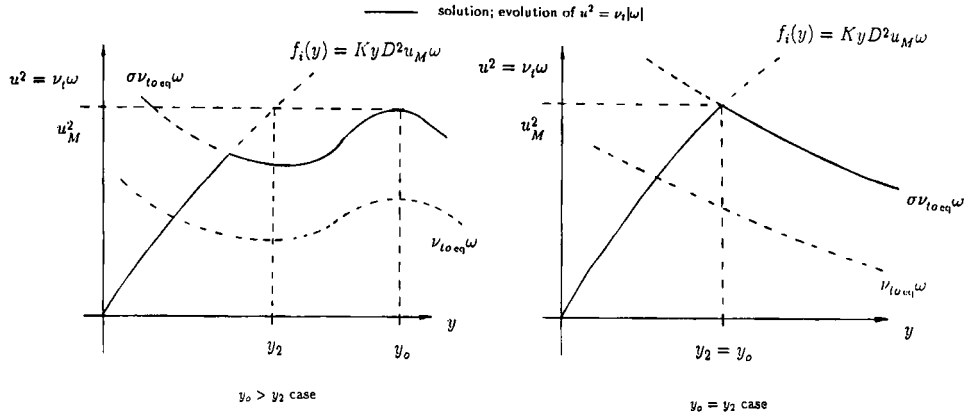

Figure 5. Determination of values of σ which enforce $u_M = \tilde{u}_M$

(40) still gives the value σ that enforces $u_M = \tilde{u}_M$ (Figure 6(a)). The second case is when $y_i > y_o$. In this case it is not possible to enforce $u_M = \tilde{u}_M$; no solution for σ exists (Figure 6(b)).

Also possible is to find a situation where an infinite number of solutions for σ exist. This interesting situation arises when $f_i(y)$ is tangent to u_M^2 for some y (Figure 7). In practice, to find that $f_i(y)$ is just tangent to u_M^2 is unlikely, but near-tangent situations were observed. These near-tangent situations usually lead to abnormal values for σ ($\sigma \gg 1$ or $\sigma \ll 1$). The appearance of

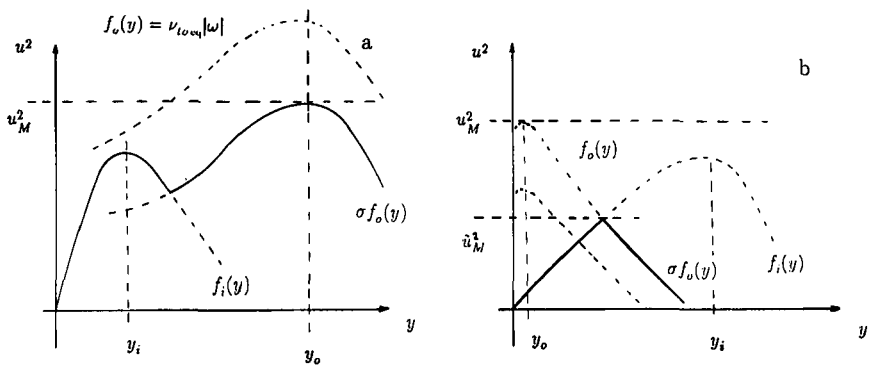

Figure 6. Illustration of situations where the function f_i does not intersect u_M^2

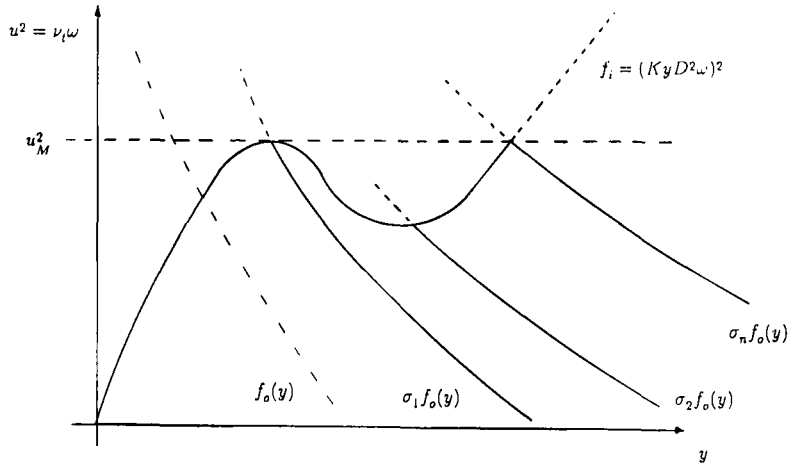

Figure 7. Case with an infinite number of solutions for σ

abnormal values can be illustrated by considering the situation where at the iterative step n the function $f_i(y)$ presents a local maximum $f_i(y_{iM})$ close to u_M^2, i.e. $f_i^{(n)}(y_{iM}) \doteq u_M^{2(n)} - \varepsilon$. Let us further assume that at the $n+1$ iterative step

$$f_i^{(n+1)}(y_{iM}) = u_M^{2(n+1)} + \varepsilon.$$

When these conditions are encountered, small values for σ will be found since equation (40) leads to

$$\sigma^{(n+1)} \ll \sigma^{(n)},$$

especially when $f_o(y)$ is a decreasing function for $y \geq y_{iM}$ (Figure 8). Similarly, large values for σ are obtained when $u_M^{(n)} = f_i^{(n)}(y_{iM}) - \varepsilon$ and $u_M^{(n+1)} = f_i^{(n+1)}(y_{iM})$. Thus, when $f_i(y)$ presents an extremum $f_i(y_{iM})$ in the range of possible values of u_M, the function $\sigma(u_M)$ will be discontinuous at $u_M^2 = f_i(y_{iM})$ and numerical difficulties should be expected. By introducing a blending between ν_{ti} and ν_{to} as

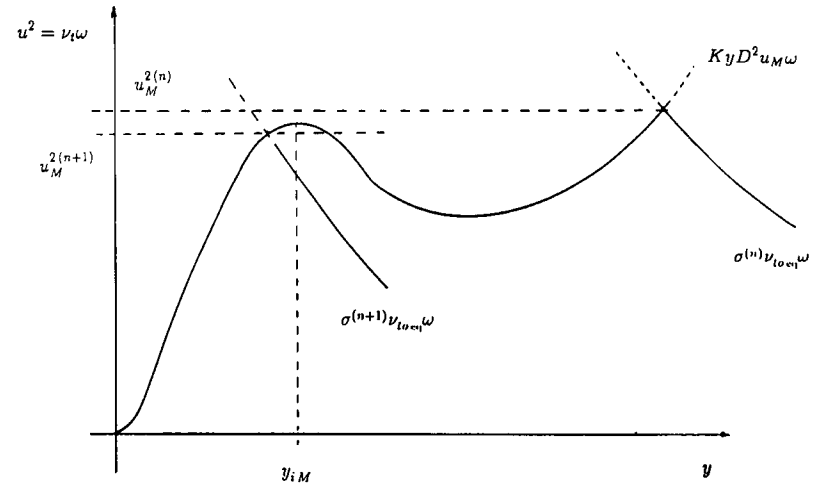

Figure 8. Illustration of a case where a small change in u_M induces a large change in σ

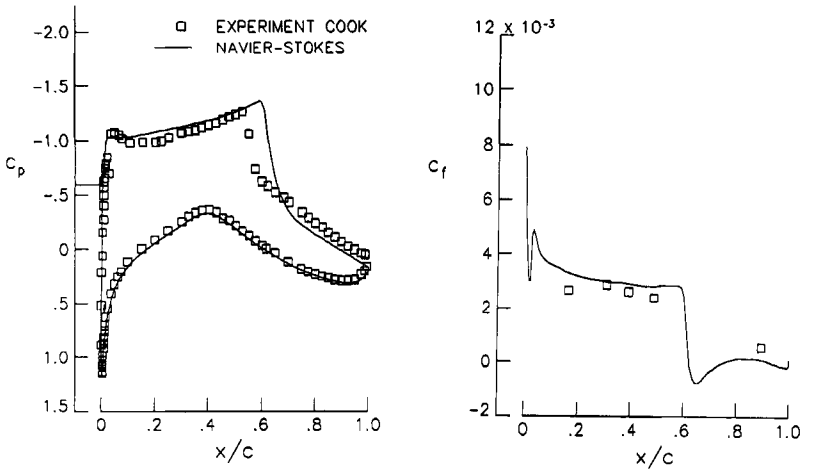

Figure 9. Pressure and skin friction distributions RAE 2822 (case 10): Baldwin–Lomax model, 257 × 65 mesh

proposed by Johnson and King, it is possible to reduce the amplitude of σ. In practice, this modification was not found to be sufficient to prevent σ from taking abnormal values. Therefore fixed bounds on σ have to be imposed.

8. RESULTS AND DISCUSSIONS

In order to validate the implementation of the Johnson–King model, computations were performed on the RAE 2822 aerofoil with $M_\infty = 0{\cdot}75$, $\alpha = 2{\cdot}81$ and $Re = 6{\cdot}2 \times 10^6$, flow conditions referred to as case 10 in Reference 22. Under these conditions a shock-induced separation forms on the upper surface of the aerofoil. In this case, as is well known, the Baldwin–Lomax turbulence model does not predict an adequate level for the eddy viscosity and the shock is located in the wrong position (Figure 9). With the Johnson–King model, excellent pressure and skin friction

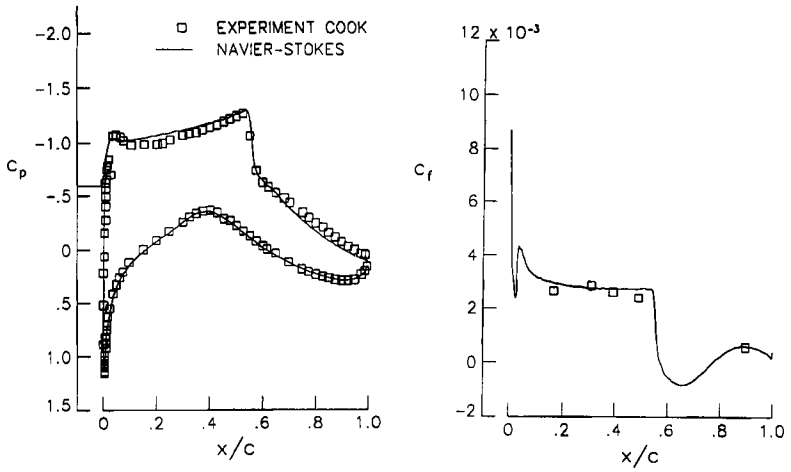

Figure 10. Pressure and skin friction distributions, RAE 2822 (case 10): Johnson–King model, 321 × 65 mesh

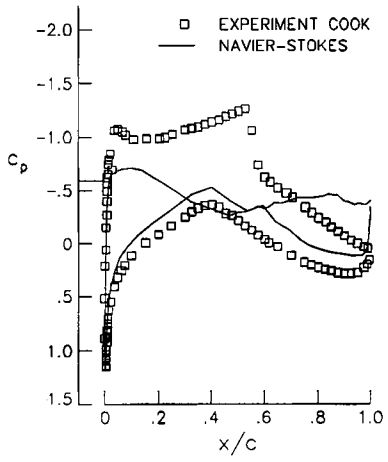

Figure 11. Pressure distribution, RAE 2822 (case 10): original Johnson–King model, 161 × 33 mesh

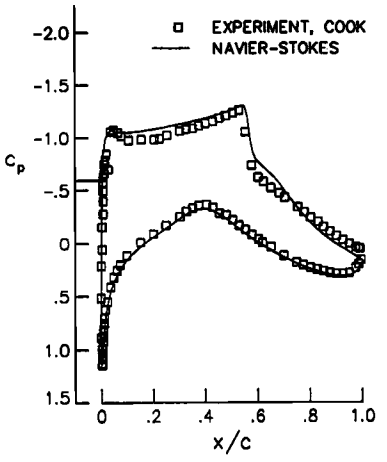

Figure 12. Pressure distribution, RAE 2822 (case 10): Johnson–King model with Baldwin–Lomax formulation for $\nu_{t_{i_{eq}}}$, 257 × 65 mesh

distributions have been found (Figure 10). However, it has been observed that the Johnson–King model is particularly sensitive to the initial level of the maximum shear stress. For instance, the 'solution' (unsteady) shown in Figure 11 has been obtained in the following manner: the Reynolds equation with the Baldwin–Lomax model is first solved on an 81 × 17 mesh; this solution is then interpolated on a 161 × 33 mesh and used as the initial condition for this finer mesh; 50 iterations are then performed on the 161 × 33 mesh with the Baldwin–Lomax model before the original Johnson–King model is turned on. If more iterations had been performed on the 161 × 33 mesh with the Baldwin–Lomax model, steady but wrong solutions would have been obtained as well. The correct solution is obtained only when the flow field is initialized with the converged flow obtained with the Baldwin–Lomax model. In order to enforce a unique solution—independent of

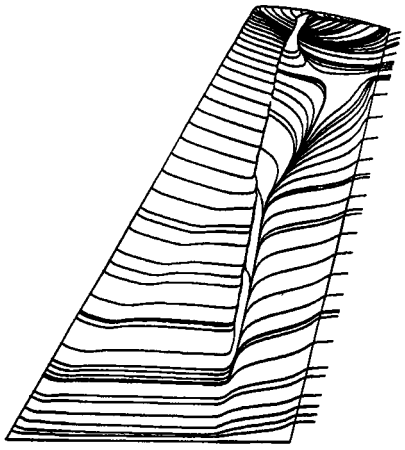

Figure 13. Wall streamlines, ONERA M6: $M_\infty = 0{\cdot}84$, $\alpha = 6{\cdot}06$, $Re = 11 \times 10^6$, Baldwin–Lomax model, $193 \times 49 \times 33$ mesh

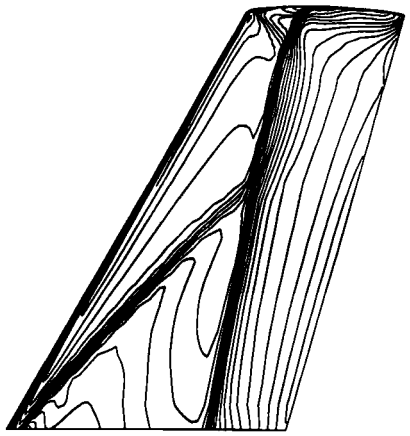

Figure 14. Pressure contours, ONERA M6: $M_\infty = 0{\cdot}84$, $\alpha = 6{\cdot}06$, $Re = 11 \times 10^6$, Baldwin–Lomax model, $193 \times 49 \times 33$ mesh

the initial condition—the velocity scale used in the inner layer of the equilibrium eddy viscosity, $\nu_{ti\,eq}$, has to be replaced. Instead of using $u_{eq} = \nu_{t\,eq}|\omega|$ as in the original Johnson–King model, $u_{eq} = \max(\nu_{t\,eq}|\omega|,\ \nu|\omega|)$ must be employed. This remedy was, however, not sufficient in the computation of the ONERA M6 wing. The level of the starting maximum shear stress was in this case still too low and, as a consequence, the shock location was moving upstream without bound. The remedy was then to replace, in the computation of $\nu_{ti\,eq}$, the inner layer formulation of Johnson and King by the Baldwin–Lomax formulation $\nu_{ti\,eq} = K^2\eta^2 D^2|\omega|$. Unfortunately, it can be observed that with the Baldwin–Lomax formulation for $\nu_{ti\,eq}$ the pressure recovery on the RAE 2822 aerofoil is not predicted as well as with the 'original' formulation; a pressure bump is found as displayed in Figure 12. The observed sensitivity of the Johnson–King model is primary due to the position of the maximum of $\nu_{t\,eq}|\omega|$ in the initial sections—where $\tau_M = \tau_{eq}$ is enforced. If the maximum is in the inner layer, then situations where a small change in u_M induces a large change in σ, as explained above, are likely to appear. In these cases the solution becomes extremely sensitive to the actual value of σ, a value highly affected by the inner layer formulation for ν_t.

For three-dimensional flows as well as for two-dimensional flows we found that if the value of σ is correctly monitored, accurate predictions of separated flows can be obtained. The test case is the ONERA M6 wing for which comparisons with experiments are possible.[23] For an angle of attack $\alpha = 6{\cdot}06$ a large separation region forms on the upper surface of the wing as shown in Figure 13. In this case the Baldwin–Lomax model is again inadequate to capture the main features of the flow. The pressure plateau after the interaction of the shocks—the shock emanating from the leading edge and the normal shock (Figure 14)—is, for instance, not captured at all. Since pressure plateau regions behind a shock wave are usually the result of a large reverse flow region, a non-equilibrium model must be used in order to obtain good resolution of the pressure distribution. With the non-equilibrium model of Johnson and King it is clear that a good representation of this pressure distribution is indeed obtained (Figure 15) and the expected large reverse flow region is effectively found (Figure 16). These results are the consequence of the lower values of eddy viscosity predicted by the Johnson–King model in adverse pressure gradient regions. The lower values of eddy viscosity also induce an upstream movement of the shock

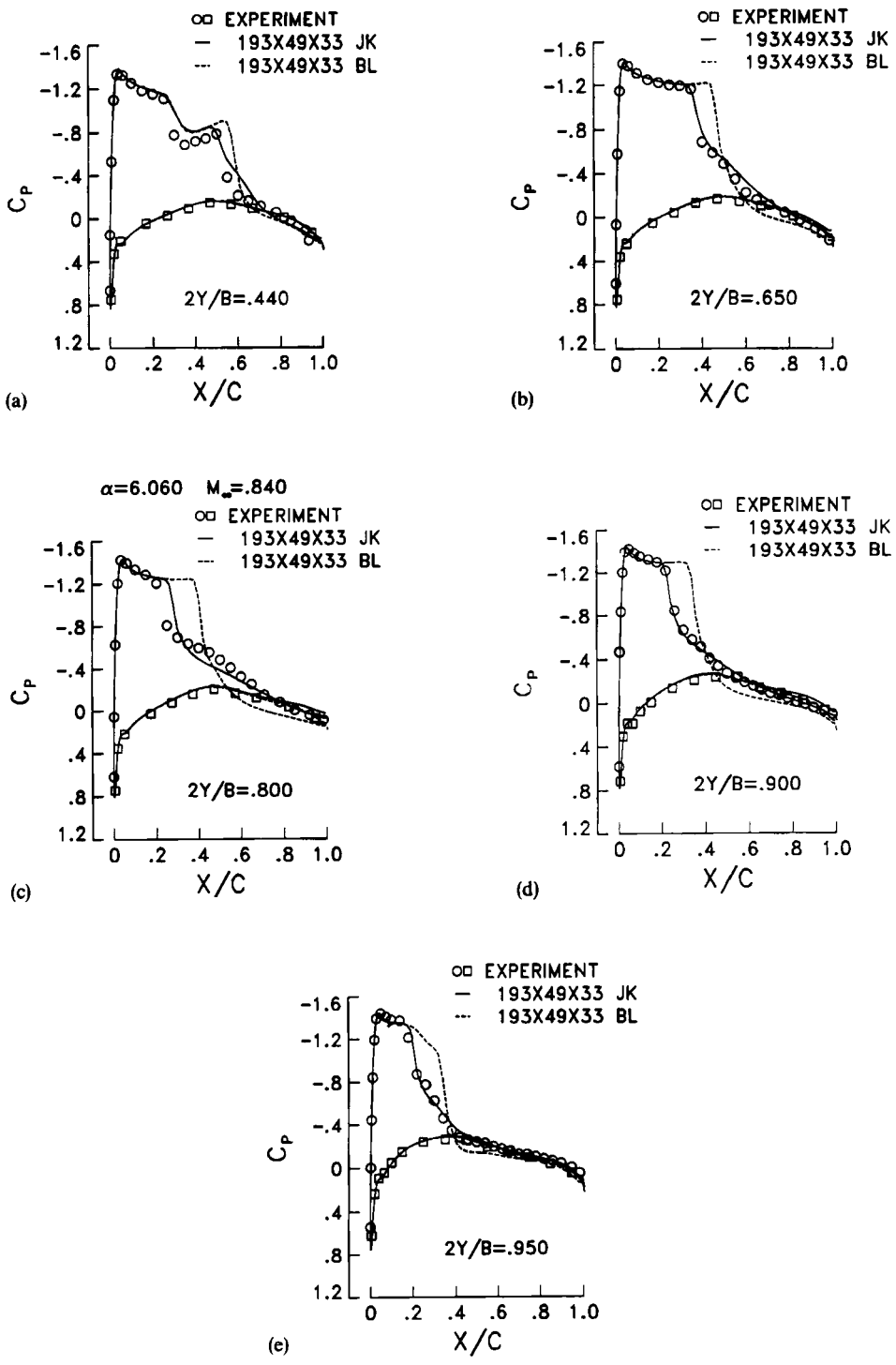

Figure 15. Pressure distributions, ONERA M6: $M_\infty = 0{\cdot}84$, $\alpha = 6{\cdot}06$, $Re = 11 \times 10^6$, Baldwin–Lomax and Johnson–King models

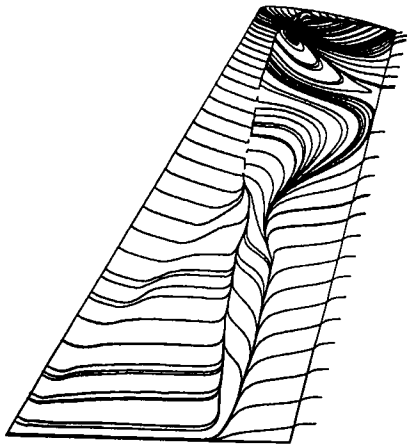

Figure 16. Wall streamlines, ONERA M6: $M_\infty = 0{\cdot}84$, $\alpha = 6{\cdot}06$, $Re = 11 \times 10^6$, Johnson–King model, $193 \times 49 \times 33$ mesh

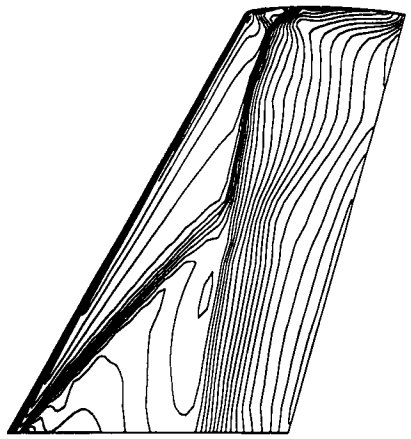

Figure 17. Pressure contours, ONERA M6: $M_\infty = 0{\cdot}84$, $\alpha = 6{\cdot}06$, $Re = 11 \times 10^6$, Johnson–King model, $193 \times 49 \times 33$ mesh

location (Figure 17). No experimental visualizations of the wall streamlines are available for the ONERA M6 wing, but these mushroom-type structures were observed experimentally on other wings.[24] For an attached flow case, $\alpha = 3{\cdot}06$, the Johnson–King model predicts a shock location which is slightly upstream of the position obtained with the Baldwin–Lomax model (Figure 18). This behaviour of the Johnson–King model has already been observed in two dimensions by Coakley.[19] Recently, Johnson and Coakley[25] modified the non-equilibrium model to improve the prediction of the model for attached flows. With the analysis of the numerical behaviour of the model described in Section 7, which explains the sensitivities of the model and gives some indications of how to control them, it is thought that the model can be used routinely for the computation of attached and separated flows of wings.

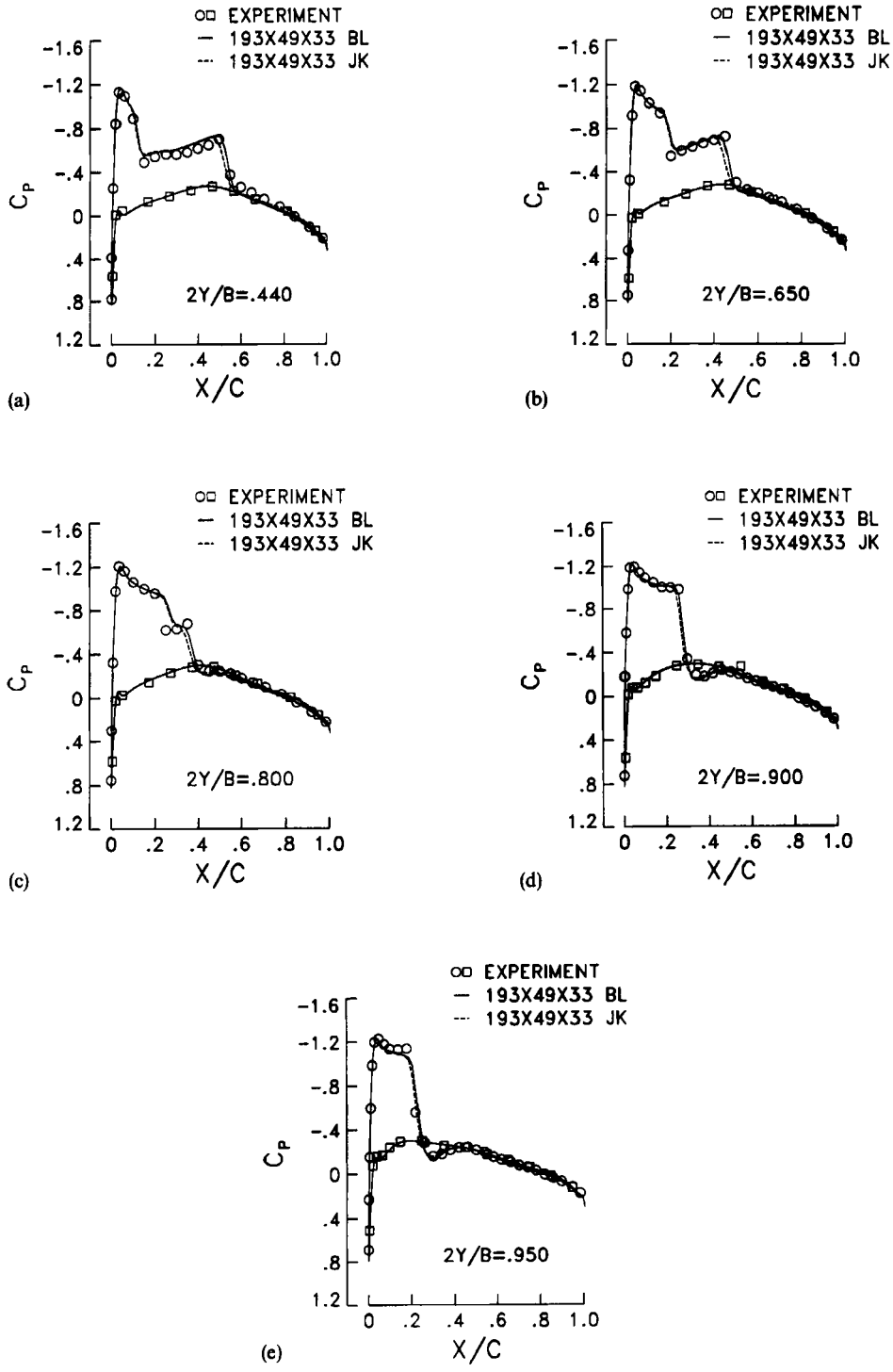

Figure 18. Pressure distributions, ONERA M6: $M_\infty = 0{\cdot}84$, $\alpha = 3{\cdot}06$, $Re = 11 \times 10^6$, Baldwin–Lomax and Johnson–King models

ACKNOWLEDGEMENTS

This work was performed at the NASA Langley Research Center, U.S.A. while the author held a National Research Council Associateship and at the ENSM, Nantes, France in the CFD Group UA1217.

REFERENCES

1. R. M. Beam and R. F. Warming, 'An implicit finite-difference algorithm for hyperbolic systems in conservation law form', *J Comput. Phys.*, **22**, 87–110 (1976).
2. A. Jameson, 'Solution of the Euler equations by a multigrid method', *Appl. Math. Comput.*, **13**, 327–356 (1983).
3. A. Jameson, W. Schmidt and E. Turkel, 'Numerical solution of the Euler equation by finite-volume methods using Runge–Kutta time-stepping', *AIAA Paper 81-1259*, 1981.
4. S. Osher, 'Shock modeling in aeronautics', in K. W. Morton and M. J. Baines (eds), *Numerical Methods for Fluid Dynamics*, Academic, New York, 1982, pp. 179–217.
5. P. L. Roe, 'Approximate Riemann solvers, parameter vectors, and difference schemes', *J. Comput. Phys.*, **43**, 357–372 (1981).
6. S. K. Godunov, 'Finite difference methods for numerical computations of discontinuous solutions of equations of fluid dynamics', *Math. Sbornik.*, **47**, 271–295 (1959).
7. B. Van Leer, 'Towards the ultimate conservative difference scheme IV. A new approach to numerical convection', *J. Comput. Phys.*, **23**, 276–298 (1977).
8. S. Chakravarthy and S. Osher, 'A new class of high accuracy TVD schemes for hyperbolic conservation laws', *AIAA Paper 85-0363*, 1985.
9. Y. P. Marx, 'Computation of turbulent flow on a CAST 10 wing using an upwind scheme', *AIAA Paper 89-1836*, 1989.
10. P. L. Roe and J. Pike, 'Efficient construction and utilisation of approximate Riemann solutions', in R. Glowinski and J.-L. Lions (eds), *Computing Methods in Applied Sciences and Engineering, Vol. 6*, North-Holland, Amsterdam, 1984, pp. 499–518.
11. T. J. Coakley, 'Implicit upwind methods for the compressible Navier–Stokes equations', *AIAA Paper 83-1958*, 1983.
12. R. W. MacCormack, 'Current status of numerical solutions of the Navier–Stokes equations', *AIAA Paper 85-0032*, 1985.
13. J. L. Thomas, B. Van Leer and R. W. Walters, 'Implicit flux-split schemes for the Euler equations', *AIAA Paper 85-1680*, 1985.
14. Y. Marx and J. Piquet, 'Comparison of implicit methods for the compressible Navier–Stokes equations', in K. W. Morton and M. J. Baines (eds), *Numerical Methods for Fluid Dynamics III*, Clarendon, Oxford, 1988, pp. 282–288.
15. S. R. Chakravarthy, 'High resolution upwind formulations for the Navier–Stokes equations', *VKI Lecture Series, 1988-05*, 1988.
16. D. S. Chaussee and T. H. Pulliam, 'A diagonal form of an implicit approximate factorization algorithm with application to a two dimensional inlet', *AIAA Paper 80-0067*, 1980.
17. J. L. Thomas and M. D. Salas, 'Far-field boundary conditions for transonic lifting solutions to the Euler equations', *AIAA Paper 85-0020*, 1985.
18. B. Baldwin and H. Lomax, 'Thin-layer approximation and algebraic model for separated turbulent flows', *AIAA Paper 78-257*, 1978.
19. T. J. Coakley, 'Numerical simulation of viscous transonic airflow flows', *AIAA Paper 87-0416*, 1987.
20. D. A. Johnson and L. S. King, 'A mathematically simple turbulence closure model for attached and separated turbulent boundary layers', *AIAA J.*, **23**, 1684–1692 (1985).
21. R. Abid, V. N. Vatsa, D. A. Johnson and B. W. Wedan, 'Prediction of separated transonic wing flows with a non-equilibrium algebraic model', *AIAA Paper 89-0558*, 1989.
22. P. H. Cook, M. A. McDonald and M. C. P. Firmin, 'Aerofoil RAE 2822—pressure distributions and boundary layer and wake measurements', *AGARD AR 138*, 1979.
23. V. Schmitt and F. Charpin, 'Pressure distributions on the ONERA-M6 wing at transonic mach numbers', *AGARD AR 138*, 1979.
24. W. K. Lockman and H. L. Seegmiller, 'An experimental investigation of the subcritical and supercritical flow about a swept semispan wing', *NASA TM 84376*, 1983.
25. D. A. Johnson and T. J. Coakley, 'Improvements to a nonequilibrium algebraic turbulence model', *AIAA J.*, **28**, 2000–2003 (1990).